
One Million Scenes for Autonomous Driving: ONCE Dataset

Jiageng Mao^{1*}Minzhe Niu^{2*}Chenhan Jiang²Hanxue Liang⁵Jingheng Chen³Xiaodan Liang^{4†}Yamin Li³Chaoqiang Ye²Wei Zhang²Zhenguo Li²Jie Yu³Hang Xu^{2†}Chunjing Xu²

Abstract

Current perception models in autonomous driving have become notorious for greatly relying on a mass of annotated data to cover unseen cases and address the long-tail problem. On the other hand, learning from unlabeled large-scale collected data and incrementally self-training powerful recognition models have received increasing attention and may become the solutions of next-generation industry-level powerful and robust perception models in autonomous driving. However, the research community generally suffered from data inadequacy of those essential real-world scene data, which hampers the future exploration of fully/semi/self-supervised methods for 3D perception. In this paper, we introduce the ONCE (One million sCenEs) dataset for 3D object detection in the autonomous driving scenario. The ONCE dataset consists of 1 million LiDAR scenes and 7 million corresponding camera images. The data is selected from 144 driving hours, which is 20x longer than the largest 3D autonomous driving dataset available (*e.g.* nuScenes and Waymo), and it is collected across a range of different areas, periods and weather conditions. To facilitate future research on exploiting unlabeled data for 3D detection, we additionally provide a benchmark in which we reproduce and evaluate a variety of self-supervised and semi-supervised methods on the ONCE dataset. We conduct extensive analyses on those methods and provide valuable observations on their performance related to the scale of used data. Data, code, and more information are available at <http://www.once-for-auto-driving.com>.

1 Introduction

Autonomous driving is a promising technology that has the potential to ease the drivers' burden and save human lives from accidents. In autonomous driving systems, 3D object detection is a crucial technique that can identify and localize the vehicles and humans surrounding the self-driving vehicle, given 3D point clouds from LiDAR sensors and 2D images from cameras as input. Recent advances [4, 40] in 3D object detection demonstrate that large-scale and diverse scene data can significantly improve the perception accuracy of 3D detectors.

Unlike other image-based datasets (*e.g.* ImageNet [12], MS COCO [27]) in which the training data can be obtained directly from websites and the annotation pipeline is relatively simple, the research community generally faces two major problems on the acquisition and exploitation of scene data for autonomous driving: 1) The data resources are scarce and the scenes generally lack diversity. The scenes for autonomous driving must be collected by driving a car that carries an expensive sensor suite

* Equal contribution.

¹ The Chinese University of Hong Kong

² Huawei Noah's Ark Lab

³ Huawei IAS BU Vehicle Cloud Service

⁴ Sun Yat-Sen University

⁵ ETH Zurich

[†] Corresponding authors: xu.hang@huawei.com & xdliang328@gmail.com



Figure 1: Images and point clouds sampled from the ONCE (One million sCenEs) dataset. Our ONCE dataset covers a variety of geographical locations, time periods and weather conditions.

on the roads in compliance with local regulations. Thus existing autonomous driving datasets could only provide a limited amount of scene data. For instance, on the largest Waymo Open dataset [40], the scene data is recorded with only 6.4 driving hours, which can hardly cover enough different circumstances. 2) Effectively leveraging unlabeled scene data becomes an important problem in practical applications. Typically a data acquisition vehicle can collect more than 200k frames of point clouds with 8 working hours, but a skilled worker can only annotate 100-200 frames per day. This will lead to a rapid accumulation of a large amount of unlabeled data. Although algorithms of semi-supervised learning [33, 41, 47], self-supervised learning [19, 18] and unsupervised domain adaptation [28, 15] show promising results to handle those unlabeled data on the image domain, currently only a few methods [44, 48] are studied for the autonomous driving scenario, mainly because of the limited data amount provided by existing datasets.

To resolve the data inadequacy problem, in this paper, we introduce the ONCE (One million sCenEs) dataset, which is the largest and most diverse autonomous driving dataset to date. The ONCE dataset contains 1 million 3D scenes and 7 million corresponding 2D images, which is 5x quantitatively more than the largest Waymo Open dataset [40], and the 3D scenes are recorded with 144 driving hours, which is 20x longer and covers more diverse weather conditions, traffic conditions, time periods and areas than existing datasets. Figure 1 shows various scenes in the ONCE dataset. Each scene is captured by a high-quality LiDAR sensor and transformed to dense 3D point clouds with 70k points per scene in average. For each scene, 7 cameras capture high-resolution images that cover 360° field of view. The data of LiDAR sensor and cameras are precisely synchronized and additional calibration and transformation parameters are provided to enable the fusion of multiple sensors and scenes. We exhaustively annotated 16k scenes with 3D ground truth boxes of 5 categories (car, bus, truck, pedestrian and cyclist), giving rise to 417k 3D boxes in total. And 769k 2D bounding boxes are also provided for camera images by projecting 3D boxes into image planes. The other scenes are kept unannotated, mainly to facilitate future research on the exploitation of unlabeled data. Comprehensive comparisons between the ONCE dataset and other autonomous driving datasets are in Table 1.

To resolve the unlabeled data exploitation problem and facilitate future research on this area, in this paper, we introduce a 3D object detection benchmark in which we implement and evaluate a variety of self-supervised and semi-supervised learning methods on the ONCE dataset. Specifically, we first carefully select a bunch of widely-used self-supervised and semi-supervised learning methods, including classic image algorithms and methods for the indoor 3D scenario. Then we adapt those methods to the task of 3D object detection for autonomous driving and reproduce their methods with the same detection framework. We train and evaluate those approaches and finally provide some observations on semi-/self-supervised learning for 3D detection by analyzing the obtained results. We also provide baseline results for multiple 3D detectors and unsupervised domain adaptation methods. Extensive experiments show that models pretrained on the ONCE dataset perform much better than those pretrained on other datasets (nuScenes and Waymo) using the same self-supervised method, which implies the superior data quality and diversity of our dataset.

| Dataset | Scenes | Size (hr.) | Area (km ²) | Images | 3D boxes | night/rain | Cls. |
|--------------------|-----------|------------|-------------------------|-----------|----------|----------------|------|
| KITTI [16] | 15k | 1.5 | - | 15k | 80k | No/No | 3 |
| ApolloScape [29] | 20k | 2 | - | 0 | 475k | No/No | 6 |
| KAIST [11] | 8.9k | - | - | 8.9k | 0 | Yes/No | 3 |
| A2D2 [17] | 40k | - | - | - | - | No/Yes | 14 |
| H3D [32] | 27k | 0.8 | - | 83k | 1.1M | No/No | 8 |
| Cityscapes 3D [14] | 20k | - | - | 20k | - | No/No | 8 |
| Argoverse [7] | 44k | 1 | 1.6 | 490k | 993k | Yes/Yes | 15 |
| Lyft L5 [21] | 30k | 2.5 | - | - | 1.3M | No/No | 9 |
| A*3D [34] | 39k | 55 | - | 39k | 230k | Yes/Yes | 7 |
| nuScenes [4] | 400k | 5.5 | 5 | 1.4M | 1.4M | Yes/Yes | 23 |
| Waymo Open [40] | 230k | 6.4 | 76 | 1M | 12M | Yes/Yes | 4 |
| ONCE (ours) | 1M | 144 | 210 | 7M | 417k | Yes/Yes | 5 |

Table 1: Comparisons with other 3D autonomous driving datasets. "-" means not mentioned. Our ONCE dataset has 4x scenes, 7x images, and 20x driving hours compared with the largest dataset [40].

Our main contributions can be summarized into two folds: 1) We introduce the ONCE dataset, which is the largest and most diverse autonomous driving dataset up to now. 2) We introduce a benchmark of self-supervised and semi-supervised learning for 3D detection in the autonomous driving scenario.

2 Related Work

Autonomous driving datasets. Most autonomous driving datasets collect data on the roads with multiple sensors mounted on a vehicle, and the obtained point clouds and images are further annotated for perception tasks including detection and tracking. The KITTI dataset [16] is a pioneering work in which they record 22 road sequences with stereo cameras and a LiDAR sensor. The ApolloScape dataset [20] offers per-pixel semantic annotations for 140k camera images and [29] additionally provides point cloud data based on the ApolloScape. The KAIST Multi-Spectral dataset [11] uses thermal imaging cameras to record scenes. The H3D dataset [32] provides point cloud data in 160 urban scenes. The Argoverse dataset [7] introduces geometric and semantic maps. The Lyft L5 dataset [21] and the A*3D dataset [34] offer 46k and 39k annotated LiDAR frames respectively.

The nuScenes dataset [4] and the Waymo Open dataset [40] are currently the most widely-used autonomous driving datasets. The nuScenes dataset records 5.5 hours driving data by multiple sensors with 400k 3D scenes in total, and the Waymo Open dataset offers 200k scenes of 6.4 driving hours with massive annotations. Compared with those two datasets, our ONCE dataset is not only quantitatively larger in terms of scenes and images, *e.g.* 1M scenes versus 200k in [40], but also more diverse since our 144 driving hours cover all time periods as well as most weather conditions. Statistical comparisons with other autonomous driving datasets are shown in Table 1.

3D object detection in driving scenarios. Many techniques have been explored for 3D object detection in driving scenarios, and they can be broadly categorized into two classes: 1) Single-modality 3D detectors [49, 36, 24, 37, 52, 58, 35, 50] are designed to detect objects solely from sparse point clouds. PointRCNN [36] operates directly on point clouds to predict bounding boxes. SECOND [49] rasterizes point clouds into voxels and applies 3D convolutional networks on voxel features to generate predictions. PointPillars [24] introduces the pillar representation to project point clouds to Bird Eye View (BEV) and utilizes 2D convolutional networks for object detection. PV-RCNN [37] combines point clouds and voxels for proposal generation and refinement. CenterPoints [52] introduces the center-based assignment scheme for accurate object localization. 2) Multi-modality approaches [43, 9, 22, 38, 26, 53] leverage both point clouds and images for 3D object detection. PointPainting [43] uses images to generate segmentation maps and appends the segmentation scores to corresponding point clouds to enhance point features. Other methods [9, 22] try to fuse point features and image features on multiple stages of a detector. Our benchmark evaluates a variety of 3D detection models, including both single-modality and multi-modality detectors on the ONCE dataset.

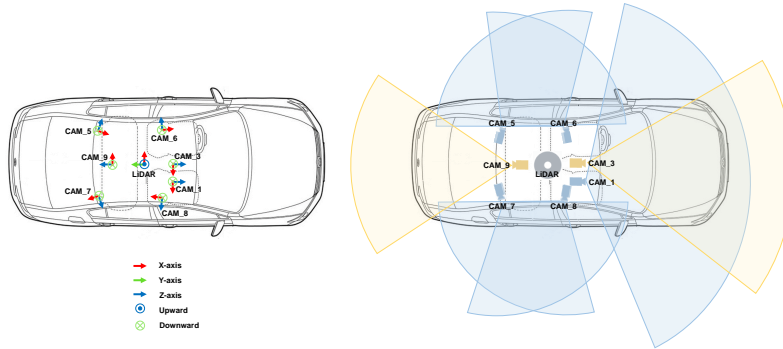


Figure 2: Sensor locations and coordinate systems. The data acquisition vehicle is equipped with 1 LiDAR and 7 cameras that can capture 3D point clouds and images from 360° field of view.

| | Freq. (Hz) | HFOV (°) | VFOV (°) | Size | Range (m) | Accuracy (cm) | Points/second |
|---------|------------|----------|------------|-----------|------------|---------------|---------------|
| CAM_1,9 | 10 | 60.6 | [-18, +18] | 1920×1020 | n/a | n/a | n/a |
| CAM_3-8 | 10 | 120 | [-37, +37] | 1920×1020 | n/a | n/a | n/a |
| LiDAR | 10 | 360 | [-25, +15] | n/a | [0.3, 200] | ±2 | 7.2M |

Table 2: Detailed parameters of LiDAR and cameras.

Deep learning on unlabeled data. Semi-supervised learning and self-supervised learning are two promising areas in which various emerging methods are proposed to learn from the unlabeled data effectively. Methods on semi-supervised learning are mainly of two branches: The first branch of methods try to annotate those unlabeled data with pseudo labels [25, 3, 2, 33] by self-training [47] or teacher model [41]. Other methods [46, 28, 23, 30, 39] regularize pairs of augmented images under consistency constraints. Self-supervised learning approaches learn from the unlabeled data by leveraging auxiliary tasks [55, 31] or by clustering [5, 6, 1]. Recent advances [19, 18, 10, 8] demonstrate that contrastive learning methods show promising results in self-supervised learning. Semi-/self-supervised learning has also been studied in 3D scenarios. SESS [57] is a semi-supervised method that utilizes geometric and semantic consistency for indoor 3D object detection. 3DIoUMatch [44] utilizes an auxiliary IoU head for boxes filtering. For self-supervised learning, PointContrast [48] and DepthContrast [56] apply contrastive learning on point clouds. Our benchmark provides a fair comparison of various self-supervised and semi-supervised methods.

3 ONCE Dataset

3.1 Data Acquisition System

Sensor specifications. The data acquisition system is built with one 40-beam LiDAR sensor and seven high-resolution cameras mounted on a car. The specific sensor layout is shown in Figure 2, and the detailed parameters of all sensors are listed in Table 2. We note that the LiDAR sensor and the set of cameras can both capture data covering 360° horizontal field of view near the driving vehicle, and all the sensors are well-synchronized, which enables good alignments of cross-modality data. We carefully calibrate the intrinsics and extrinsics of each camera using calibration target boards with patterns. We check the calibration parameters every day and re-calibrate the sensor that has errors. We make the intrinsics and extrinsics public along with the data to users for camera projection.

Data collection and annotation. The data was collected in multiple cities in China. We conform to the local regulations and avoid releasing specific city names and locations. The data collection process lasts 3 months. 3D ground truth boxes were manually labeled from point clouds by annotators

using a commercial annotation system. The labeled boxes then went through a double-check process for validness and refinement, which guarantees high-quality bounding boxes for 3D object detection.

Data protection. The driving scenes are collected in permitted areas. We comply with the local regulations and avoid releasing any localization information including GPS information and map data. For privacy protection, we actively detect any object on each image that may contain personal information, *e.g.* human faces, license plates, with a high recall rate, and then we blur those detected objects to ensure no personal information is disclosed.

3.2 Data Format

Coordinate systems. There are 3 types of coordinate systems on the ONCE dataset, *i.e.*, the LiDAR coordinate, the camera coordinates, and the image coordinate. The LiDAR coordinate is placed at the center of the LiDAR sensor, with the x-axis positive to the left, the y-axis positive backwards, and the z-axis positive upwards. We additionally provide a transformation matrix (vehicle pose) between current frame and the first frame, which enables the fusion of multiple point clouds. The camera coordinates are placed at the center of the lens respectively, with the x-y plane parallel to the image plane and the z-axis positive forwards. The camera coordinates can be transformed to the LiDAR coordinate directly using the respective camera extrinsics. The image coordinate is a 2D coordinate system where the origin is at the top-left of the image, and the x-axis and the y-axis are along the image width and height respectively. The camera intrinsics enable the projection from the camera coordinate to the image coordinate. An illustration of our coordinate systems is in Figure 2.

LiDAR data. The original LiDAR data is recorded at a speed of 10 frames per second (FPS). We further downsample those original data with the sampling rate of 2 FPS, since most adjacent frames are quite similar thus redundant. The downsampled data is then transformed into 3D point clouds, resulting in 1 million point clouds, *i.e.*, scenes in total. Each point cloud is represented as an $N \times 4$ matrix, where N is the number of points in this scene, and each point is a 4-dim vector (x, y, z, r) . The 3D coordinate (x, y, z) is based on the LiDAR coordinate, and r denotes the reflection intensity. The point clouds are stored into separate binary files for each scene and can be easily read by users.

Camera data. The camera data is also downsampled along with the LiDAR data for synchronization, and then the distortions are removed to enhance the quality of the images. We finally provide JPEG compressed images for all the cameras, resulting in 7 million images in total.

Annotation format. We select 16k most representative scenes and exhaustively annotate all the 3D bounding boxes of 5 categories: car, bus, truck, pedestrian and cyclist. Each bounding box is a 3D cuboid and can be represented as a 7-dim vector: $(cx, cy, cz, l, w, h, \theta)$, where (cx, cy, cz) is the center of the cuboid on the LiDAR coordinate, (l, w, h) denotes length, width, height, and θ is the yaw angle of the cuboid. We provide 2D bounding boxes by projecting 3D boxes on image planes.

Other information. Weather and time information of each scene is useful since it contains explicit domain knowledge, but existing datasets seldom release those important data. In the ONCE dataset, we provide 3 weather conditions, *i.e.*, sunny, cloudy, rainy, and 4 time periods, *i.e.*, morning, noon, afternoon, night, for every labeled and unlabeled scene. We pack all the information, *i.e.*, weather, period, timestamp, pose, calibration, annotations, into a single JSON file for each scene.

Dataset splits. The ONCE dataset contains 581 sequences in total. We carefully select and annotate 6 sequences (5k scenes) captured in sunny days as the training split, 4 sequences (3k scenes in total. 1 sequence collected in a sunny day, 1 in a rainy day, 1 in a sunny night and 1 in a rainy night) as the validation split, 10 sequences (8k scenes in total. 3 sequences in sunny days, 3 in rainy days, 2 in sunny nights and 2 in rainy nights) as the testing split. We note that the sequences in each split can cover both downtown and suburban areas. The validation and testing split have quite similar data distributions, and the training split has a slight domain shift compared to the validation/testing split. We choose this way mainly to encourage the proposed methods to have better generalizability.

One major goal of the ONCE dataset is to facilitate research on leveraging large-scale unlabeled data. Thus we keep the remaining 560 sequences as unlabeled, and those sequences can be used for semi-supervised and self-supervised 3D object detection. To explore the effects of different data amounts used for 3D detection, we also divide the unlabeled scenes into 3 subsets: U_{small} , U_{medium} and U_{large} . The small unlabeled set U_{small} contains 70 sequences (100k scenes), the medium set U_{medium} contains 321 sequences (500k scenes) and the large set U_{large} contains 560 sequences

| pretrain / downstream | KITTI (moderate mAP) | nuScenes (NDS) | Waymo (L2 mAP) |
|-----------------------|----------------------|----------------|----------------|
| nuScenes→ | 66.1 | - | 53.9 |
| Waymo→ | 66.5 | 49.9 | - |
| ONCE→ | 67.2 | 51.5 | 54.4 |

Table 3: Quality analysis. The model pretrained on the ONCE dataset shows superior performance compared to those on the nuScenes and Waymo dataset, which implies our superior data quality.

| | Time | Weather | Area |
|--------------|---|---|--|
| Waymo [40] | daytime (80.79%); dawn (9.04%); night (10.17%) | sunny (99.40%); rainy (0.60%) | only city-level labels |
| nuScenes [4] | daytime (88.32%); night (11.68%) | sunny (80.47%); rainy (19.53%) | only city-level labels |
| BDD100k [54] | daytime (52.57%); dawn (7.27%); night (39.94%); undefined (0.22%) | clear (53.45%); overcast (12.53%); partly cloudy (7.04%); rainy (7.27%); snowy (7.91%); foggy (0.18%); undefined (11.61%) | city street (62.14%); highway (24.89%); residential (11.68%); parking lot (0.53%); tunnel (0.20%); gas stations (0.04%); undefined (0.52%) |
| ONCE | morning (39.34%); noon (3.76%); afternoon (36.67%); night (20.24%) | sunny (63.8%); cloudy (30.09%); rainy (6.11%) | downtown (34.29%); suburbs (50.98%); tunnel (1.83%); highway (11.87%); bridge (1.02%) |

Table 4: Diversity analysis. Time and weather labels on nuScenes and Waymo are extracted from scene descriptions and annotations respectively. Both two datasets only provide city-level labels instead of specific road types. Compared to other datasets, our ONCE dataset contains sufficient data captured in rainy days and at nights, and we additionally provide the label of road type for each scene.

(about 1M scenes) in total. We note that $U_{small} \subset U_{medium} \subset U_{large}$ and U_{small}, U_{medium} are created by selecting particular roads in time order instead of uniformly sampling from all the scenes, which is more practical since the driving data is usually incrementally updated in real applications.

3.3 Dataset Analysis

Quality analysis. In order to evaluate the data quality and provide a fair comparison across different datasets, we propose an approach that utilizes pretrained models to imply the respective data quality. Specifically, we first pretrain 3 same backbones of the SECOND detector [49] by the self-supervised method DeepCluster [5] using data from nuScenes [4], Waymo [40] and ONCE respectively, and then we finetune those pretrained models on multiple downstream datasets under the same settings and report their performances. The superior model should have the best pretrained backbone, which means its corresponding pretraining dataset has the best data quality. Table 3 shows the final results. The model pretrained on the ONCE dataset attains 67.2% moderate mAP on the downstream KITTI [16] dataset, and significantly outperforms models pretrained on the Waymo dataset (66.5%) and nuScenes dataset (66.1%), which implies our superior data quality compared to nuScenes and Waymo.

Diversity analysis. We analyze the ratios of different weather conditions, time periods and areas in the ONCE dataset and compare them to those in other datasets in Table 4. Our ONCE dataset contains more rainy scenes which accounts for 20% of the total scenes, compared to 10% in Waymo and 12% in nuScenes. The ONCE dataset also provides a sufficient amount of data captured at night with 6% of the total scenes. It is worth noting that we provide explicit labels of both time, weather,

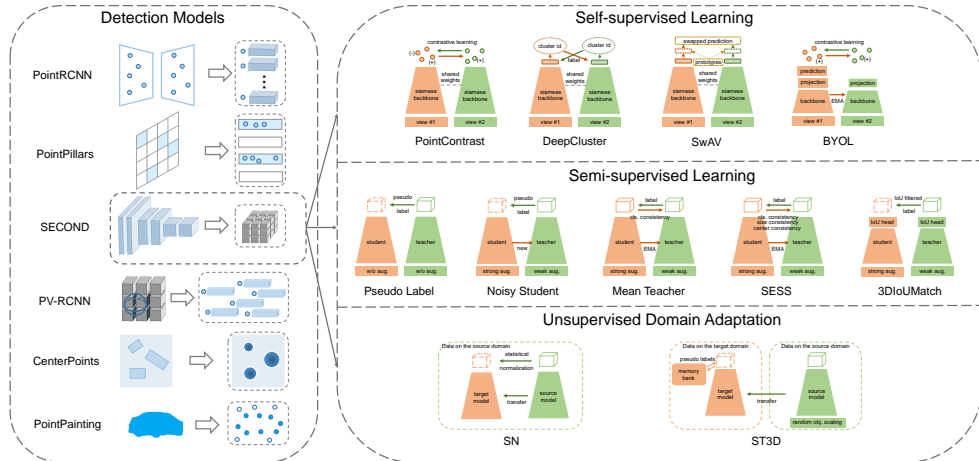


Figure 3: An overview of our 3D object detection benchmark. We reproduce 6 detection models, 4 self-supervised learning, 5 semi-supervised learning, and 2 unsupervised domain adaptation methods for 3D object detection. We give comprehensive analyses on the results and offer valuable observations.

and area for each scene, while Waymo and nuScenes didn't provide labels of collecting areas. The driving scenes can cover most road types including downtown, suburb, highway, bridge and tunnel.

4 Benchmark for 3D Object Detection

In this section, we present a 3D object detection benchmark on the ONCE dataset. We reproduce widely-used detection models as well as various methods of self-supervised learning, semi-supervised learning and unsupervised domain adaptation on 3D object detection. We validate those methods with a unified standard and provide performance analysis as well as suggestions for future research.

4.1 Models for 3D Object Detection

We implement 5 most widely-used single-modality 3D detectors: PointRCNN [36], PointPillars [24], SECOND [49], PV-RCNN [37] and CenterPoints [52] using only point clouds as input, as well as 1 multi-modality detector PointPainting [43] using both point clouds and images as input on the ONCE dataset. We train those detectors on the training split and report the overall and distance-wise AP_{3D}^{Ori} on the testing split using the evaluation metric in appendix E. Performance on the validation split is also reported in appendix B. We provide training and implementation details in appendix C.

Points vs. voxels vs. pillars. Multiple representations (points/voxels/pillars) have been explored for 3D detection. Our experiments in Table 5 demonstrate that the point-based detector [36] performs poorly with only 31.8% mAP on the ONCE dataset, since small objects like pedestrians are naturally sparse and a small amount of used points cannot guarantee a high recall rate. The voxel-based detector [49] shows decent performance with 51.90% mAP compared with 45.47% mAP of the pillar-based detector [24]. It is mainly because voxels contain finer geometric information than pillars. PV-RCNN [37] combines both the point representation and the voxel representation and further improves the detection performance to 53.85% mAP.

Anchor assignments vs. center assignments. The only difference between SECOND [49] and CenterPoints [52] is that SECOND uses anchor-based target assignments while CenterPoints introduces the center-based assignments. SECOND shows better performance on the vehicle category (69.71% vs. 66.35%) while CenterPoints performs much better on the small objects including pedestrians (51.80% vs. 26.09%) and cyclists (65.57% vs. 59.92%) in our experiments. It is because the center-based method shows stronger localization ability which is required for detecting small objects, while the anchor-based method can estimate the size of objects more precisely.

Single-modality vs. multi-modality. PointPainting [43] appends the segmentation scores to the input point clouds of CenterPoints [52], but the performance drops from 61.24% to 59.78%. We find

| Method | Vehicle | | | | Pedestrian | | | | Cyclist | | | | mAP |
|--|---------|-------|--------|---------|------------|-------|--------|---------|---------|-------|--------|---------|-------|
| | overall | 0-30m | 30-50m | 50m-inf | overall | 0-30m | 30-50m | 50m-inf | overall | 0-30m | 30-50m | 50m-inf | |
| Multi-Modality (point clouds + images) | | | | | | | | | | | | | |
| PointPainting [43] | 66.46 | 83.70 | 56.89 | 40.74 | 47.62 | 58.95 | 39.33 | 23.34 | 65.27 | 73.48 | 61.53 | 43.90 | 59.78 |
| Single-Modality (point clouds only) | | | | | | | | | | | | | |
| PointRCNN [36] | 52.00 | 74.44 | 40.72 | 22.14 | 8.73 | 12.20 | 6.96 | 2.96 | 34.02 | 46.48 | 27.39 | 11.45 | 31.58 |
| PointPillars [24] | 69.52 | 84.51 | 60.55 | 45.72 | 17.28 | 20.21 | 15.06 | 11.48 | 49.63 | 60.15 | 42.43 | 27.73 | 45.47 |
| SECOND [49] | 69.71 | 86.96 | 60.22 | 43.02 | 26.09 | 30.52 | 24.63 | 14.19 | 59.92 | 70.54 | 54.89 | 34.34 | 51.90 |
| PV-RCNN [37] | 76.98 | 89.89 | 69.35 | 55.52 | 22.66 | 27.23 | 21.28 | 12.08 | 61.93 | 72.13 | 56.64 | 37.23 | 53.85 |
| CenterPoints [52] | 66.35 | 83.65 | 56.74 | 41.57 | 51.80 | 62.80 | 45.41 | 24.53 | 65.57 | 73.02 | 62.85 | 44.77 | 61.24 |

Table 5: Results of detection models on the testing split.

| Method | Vehicle | | | | Pedestrian | | | | Cyclist | | | | mAP |
|--------------------|---------|-------|--------|---------|------------|-------|--------|---------|---------|-------|--------|---------|---------------|
| | overall | 0-30m | 30-50m | 50m-inf | overall | 0-30m | 30-50m | 50m-inf | overall | 0-30m | 30-50m | 50m-inf | |
| baseline [49] | 69.71 | 86.96 | 60.22 | 43.02 | 26.09 | 30.52 | 24.63 | 14.19 | 59.92 | 70.54 | 54.89 | 34.34 | 51.90 |
| U_{small} | | | | | | | | | | | | | |
| BYOL [18] | 67.57 | 84.61 | 58.26 | 41.59 | 17.22 | 19.45 | 16.71 | 10.43 | 53.36 | 64.95 | 47.47 | 27.66 | 46.05 (-5.85) |
| PointContrast [48] | 71.53 | 87.02 | 62.37 | 47.23 | 22.68 | 26.33 | 21.58 | 12.98 | 58.04 | 70.01 | 51.74 | 31.69 | 50.75 (+1.15) |
| SwAV [6] | 72.25 | 87.20 | 63.38 | 48.93 | 25.11 | 29.32 | 23.50 | 14.13 | 60.67 | 70.90 | 55.91 | 35.39 | 52.68 (+0.78) |
| DeepCluster [5] | 72.06 | 87.09 | 63.09 | 48.78 | 27.56 | 32.21 | 26.60 | 13.61 | 50.30 | 70.33 | 55.82 | 35.89 | 53.31 (+1.41) |
| U_{medium} | | | | | | | | | | | | | |
| BYOL [18] | 69.69 | 84.83 | 60.41 | 46.05 | 27.31 | 32.58 | 24.60 | 13.69 | 57.22 | 69.57 | 51.07 | 29.15 | 51.41 (-0.49) |
| PointContrast [48] | 70.15 | 86.71 | 61.12 | 48.11 | 29.23 | 35.52 | 36.28 | 13.06 | 58.91 | 70.05 | 53.86 | 34.27 | 52.76 (+0.86) |
| SwAV [6] | 72.10 | 87.11 | 63.15 | 48.58 | 28.00 | 33.10 | 25.88 | 14.19 | 60.17 | 70.46 | 55.61 | 34.84 | 53.42 (+1.52) |
| DeepCluster [5] | 72.12 | 87.31 | 62.97 | 48.55 | 30.06 | 36.07 | 27.23 | 13.47 | 60.45 | 70.81 | 54.93 | 36.03 | 54.21 (+2.31) |
| U_{large} | | | | | | | | | | | | | |
| BYOL [18] | 72.23 | 87.30 | 63.13 | 48.31 | 23.62 | 27.10 | 22.14 | 13.47 | 60.45 | 70.82 | 55.31 | 35.65 | 52.10 (+0.20) |
| PointContrast [48] | 73.15 | 83.92 | 67.29 | 50.97 | 27.48 | 31.45 | 24.17 | 16.70 | 58.33 | 70.37 | 52.26 | 35.61 | 52.99 (+1.09) |
| SwAV [6] | 71.96 | 86.92 | 62.83 | 48.85 | 30.60 | 36.42 | 28.03 | 14.52 | 60.27 | 70.43 | 55.52 | 36.25 | 54.28 (+2.38) |
| DeepCluster [5] | 71.85 | 86.96 | 62.91 | 48.54 | 30.54 | 37.08 | 27.55 | 13.86 | 60.42 | 70.60 | 55.47 | 36.29 | 54.27 (+2.37) |

Table 6: Results of self-supervised learning methods on the testing split.

that the performance of PointPainting heavily relies on the accuracy of segmentation scores, and without explicit segmentation labels on the ONCE dataset, we cannot generate accurate semantic segmentation maps from images, which brings negative effects on 3D detection.

4.2 Self-Supervised Learning for 3D Object Detection

We reproduce 4 self-supervised learning methods, including 2 contrastive learning methods (PointContrast [48] and BYOL [18]), as well as 2 clustering-based methods (DeepCluster [5] and SwAV [6]) on our dataset. We choose the backbone of the SECOND detector [49] as the pretrained backbone. We first pretrain the backbone using self-supervised learning methods with different amounts of unlabeled data: 100k U_{small} , 500k U_{medium} and 1 million U_{large} , and then we finetune the detection model on the training split. We report the detection performances on the testing split using the evaluation metric in appendix E. Performance on the validation split is also reported in appendix B. We provide training and implementation details in appendix C.

Self-supervised learning on unlabeled data. Experiments in Table 6 show that self-supervised methods can improve the detection results with enough unlabeled data. PointContrast [48] obtains 50.75% mAP with 100k unlabeled data, but the performance consistently improves to 52.76% and 52.99% with 500k and one million unlabeled data respectively, giving rise to 1.09% final performance gain over baseline. Self-supervised learning benefits from the increasing amount of unlabeled data.

Contrastive learning vs. clustering. The detection results indicate that clustering-based methods [5, 6] consistently outperforms contrastive learning methods [48, 18]. SwAV [6] and DeepCluster [5] achieve 54.28% and 54.27% mAP respectively on U_{large} , compared with 52.10% and 52.99% obtained by BYOL [18] and PointContrast [48]. This is mainly because constructing representative views of a 3D scene for contrastive learning is non-trivial in driving scenarios. Generating different views simply by performing different augmentations on the same point cloud may result in quite similar views that will make the pretraining process easily converge to a trivial solution.

| Method | Vehicle | | | | Pedestrian | | | | Cyclist | | | | mAP |
|---------------------------|---------|-------|--------|---------|------------|-------|--------|---------|---------|-------|--------|---------|---------------|
| | overall | 0-30m | 30-50m | 50m-inf | overall | 0-30m | 30-50m | 50m-inf | overall | 0-30m | 30-50m | 50m-inf | |
| baseline [49] | 69.71 | 86.96 | 60.22 | 43.02 | 26.09 | 30.52 | 24.63 | 14.19 | 59.92 | 70.54 | 54.89 | 34.34 | 51.90 |
| <i>U_{small}</i> | | | | | | | | | | | | | |
| Pseudo Label [25] | 71.05 | 86.51 | 61.81 | 47.49 | 25.58 | 31.03 | 22.03 | 14.12 | 58.08 | 68.50 | 52.63 | 35.61 | 51.57 (-0.33) |
| Noisy Student [47] | 73.25 | 88.84 | 64.61 | 49.95 | 28.04 | 34.62 | 23.43 | 14.20 | 57.58 | 67.77 | 53.43 | 33.76 | 52.96 (+1.06) |
| Mean Teacher [41] | 74.13 | 89.34 | 65.28 | 50.91 | 31.66 | 37.44 | 29.90 | 14.61 | 62.69 | 71.88 | 59.22 | 39.45 | 56.16 (+4.26) |
| SESS [57] | 72.42 | 87.23 | 63.55 | 49.11 | 27.32 | 32.26 | 24.47 | 15.36 | 61.76 | 72.39 | 57.29 | 37.33 | 53.83 (+1.93) |
| 3DIoUMatch [44] | 72.12 | 87.05 | 63.65 | 50.35 | 31.41 | 38.56 | 27.62 | 14.25 | 59.46 | 69.53 | 54.82 | 36.18 | 54.33 (+2.43) |
| <i>U_{medium}</i> | | | | | | | | | | | | | |
| Pseudo Label [25] | 70.72 | 86.21 | 61.72 | 47.39 | 21.74 | 25.73 | 19.91 | 13.28 | 56.01 | 67.14 | 50.18 | 33.23 | 49.49 (-2.41) |
| Noisy Student [47] | 73.97 | 89.09 | 65.35 | 51.04 | 30.32 | 36.24 | 27.08 | 16.24 | 61.35 | 71.28 | 56.70 | 37.96 | 55.22 (+3.32) |
| Mean Teacher [41] | 74.71 | 89.28 | 66.10 | 52.90 | 36.03 | 42.97 | 33.29 | 18.70 | 64.88 | 74.05 | 60.80 | 42.63 | 58.54 (+6.64) |
| SESS [57] | 72.60 | 87.02 | 64.29 | 50.68 | 35.23 | 42.59 | 31.40 | 16.64 | 64.67 | 73.93 | 61.14 | 40.80 | 57.50 (+5.60) |
| 3DIoUMatch [44] | 74.26 | 89.08 | 66.11 | 53.03 | 33.91 | 41.02 | 30.07 | 16.15 | 61.30 | 71.29 | 56.49 | 38.13 | 56.49 (+4.59) |
| <i>U_{large}</i> | | | | | | | | | | | | | |
| Pseudo Label [25] | 70.29 | 85.94 | 61.18 | 46.66 | 21.85 | 25.83 | 20.22 | 12.75 | 55.72 | 66.96 | 50.29 | 32.92 | 49.29 (-2.61) |
| Noisy Student [47] | 74.50 | 89.23 | 67.11 | 53.15 | 33.28 | 40.20 | 28.89 | 17.50 | 62.05 | 71.76 | 57.53 | 39.32 | 56.61 (+4.71) |
| Mean Teacher [41] | 76.60 | 89.41 | 68.29 | 55.66 | 36.37 | 43.84 | 32.49 | 17.11 | 66.99 | 75.87 | 63.35 | 44.06 | 59.99 (+8.09) |
| SESS [57] | 74.52 | 88.97 | 66.32 | 52.47 | 36.29 | 43.53 | 33.15 | 16.68 | 65.52 | 74.63 | 62.67 | 41.91 | 58.78 (+6.88) |
| 3DIoUMatch [44] | 74.48 | 89.13 | 66.35 | 54.59 | 35.74 | 43.35 | 32.08 | 17.34 | 62.06 | 71.86 | 58.00 | 39.09 | 57.43 (+5.53) |

Table 7: Results of semi-supervised learning methods on the testing split.

4.3 Semi-Supervised Learning for 3D Object Detection

We implement 3 image-based semi-supervised methods: Pseudo Label [25], Mean Teacher [41] and Noisy Student [47], as well as 2 semi-supervised methods for point clouds in the indoor scenario: SESS [57] and 3DIoUMatch [44]. We first pretrain the model on the training split and then apply the 5 semi-supervised learning methods on both the training split and unlabeled scenes. We train those methods with 5 epochs for the 100k unlabeled subset U_{small} , 3 epochs for the 500k subset U_{medium} and the 1 million subset U_{large} during the semi-supervised learning process. We report detection performances on the testing split with the use of unlabeled subsets U_{small} , U_{medium} and U_{large} separately. Performance on the validation split is also reported in appendix B. We provide training and implementation details in appendix C.

Semi-supervised learning on unlabeled data. Experiments in Table 7 show that most semi-supervised methods can improve the detection results using unlabeled data. For instance, Mean Teacher [41] improves the baseline result by 8.09% in mAP using the largest unlabeled set U_{large} . The detection performance can be further boosted when the amount of unlabeled data increases. SESS [57] obtains 1.93% performance gain using 100k unlabeled scenes, and the performance gain reaches 5.60% with 500k unlabeled scenes and 6.88% with one million scenes.

Pseudo labels vs. consistency. There are two keys to the success of labeling-based methods [25, 47, 44]: augmentations and label quality. Without strong augmentations, the performance of Pseudo Label [25] drops from 51.90% to 49.29% albeit one million scenes U_{large} are provided for training. 3DIoUMatch [44] adds additional step to filter out labels of low quality, and the performance reaches 57.43% compared with 56.61% of Noisy Student on U_{large} . Consistency-based methods [41, 57] generally perform better than labeling-based methods, and Mean Teacher obtains the highest performance 59.99% on U_{large} . SESS [57] performs worse than Mean Teacher with 58.78% mAP, which indicates that size and center consistency may not be useful in driving scenarios.

Semi-supervised learning vs. self-supervised learning. Our results in Table 6 and Table 7 demonstrate that the semi-supervised methods generally have a better performance compared with the self-supervised methods. Mean Teacher [41] attains the best performance of 59.99% mAP while the best self-supervised method SwAV [6] only obtains 54.28% on U_{large} . The major reason is that in semi-supervised learning the model usually receives stronger and more precise supervisory signals, e.g. labels or consistency with a trained model, when learning from the unlabeled data. However, in self-supervised learning, the supervisory signals on the unlabeled data are cluster id or similarity of pairs, which are typically noisy and uncertain.

4.4 Unsupervised Domain Adaptation for 3D Object Detection

Unsupervised domain adaptation for 3D object detection aims to adapt a detection model from the source dataset to the target dataset without supervisory signals on the target domain. Different datasets

| Task | Waymo \rightarrow ONCE | | nuScenes \rightarrow ONCE | | ONCE \rightarrow KITTI | |
|-------------|--------------------------|----------------|-----------------------------|---------------|--------------------------|----------------|
| Method | AP_{BEV} | AP_{3D} | AP_{BEV} | AP_{3D} | AP_{BEV} | AP_{3D} |
| Source Only | 65.55 | 32.88 | 46.85 | 23.74 | 42.01 | 12.11 |
| SN [45] | 67.97 (+2.42) | 38.25 (+5.67) | 62.47 (+15.62) | 29.53 (+5.79) | 48.12 (+6.11) | 21.12 (+9.01) |
| ST3D [51] | 68.05 (+2.50) | 48.34 (+15.46) | 42.53 (-4.32) | 17.52 (-6.22) | 86.89 (+44.88) | 41.42 (+29.31) |
| Oracle | 89.00 | 77.50 | 89.00 | 77.50 | 83.29 | 73.45 |

Table 8: Results on unsupervised domain adaptation. Source Only means trained on the source and directly evaluated on the target domain. Oracle means trained and tested both on the target domain.

typically have different collected environments, sensor locations and point cloud densities. In this paper, we reproduce 2 commonly-used methods: SN [45] and ST3D [51]. We follow the settings of those methods and conduct experiments on transferring the model trained on the nuScenes and Waymo Open dataset to our ONCE dataset, as well as transferring the model trained on the ONCE dataset to the KITTI dataset. The detection results of the car class are reported on the respective target validation or testing set using the KITTI AP_{3D} metric following [45, 51].

Statistical normalization vs. self-training. The normalization-based method SN [45] surpasses the Source Only model by 2.42% in AP_{BEV} and 5.67% in AP_{3D} on the Waymo \rightarrow ONCE adaptation task, and the self-training method ST3D [51] also attains a considerable performance gain with 15.46% AP_{3D} improvement. However, ST3D performs poorly on the nuScenes \rightarrow ONCE task. It is mainly because the nuScenes dataset has fewer LiDAR beams, and the model trained on nuScenes may produce more low-quality pseudo labels, which will harm the self-training process of ST3D. Although those two methods achieve strong results on the adaptation from/to the ONCE dataset, there is still a gap with the Oracle results, leaving large space for future research.

5 Conclusion

In this paper, we introduce the ONCE (One millioN sCenEs) dataset, which is the largest autonomous driving dataset to date. To facilitate future research on 3D object detection, we additionally provide a benchmark for detection models and methods of self-supervised learning, semi-supervised learning and unsupervised domain adaptation. For future works, we plan to support more tasks on autonomous driving, including 2D object detection, 3D semantic segmentation and planning.

References

- [1] Yuki Markus Asano, Christian Rupprecht, and Andrea Vedaldi. Self-labelling via simultaneous clustering and representation learning. *arXiv preprint arXiv:1911.05371*, 2019.
- [2] David Berthelot, Nicholas Carlini, Ekin D Cubuk, Alex Kurakin, Kihyuk Sohn, Han Zhang, and Colin Raffel. Remixmatch: Semi-supervised learning with distribution alignment and augmentation anchoring. *arXiv preprint arXiv:1911.09785*, 2019.
- [3] David Berthelot, Nicholas Carlini, Ian Goodfellow, Nicolas Papernot, Avital Oliver, and Colin Raffel. Mixmatch: A holistic approach to semi-supervised learning. *arXiv preprint arXiv:1905.02249*, 2019.
- [4] Holger Caesar, Varun Bankiti, Alex H Lang, Sourabh Vora, Venice Erin Liong, Qiang Xu, Anush Krishnan, Yu Pan, Giancarlo Baldan, and Oscar Beijbom. nuscenes: A multimodal dataset for autonomous driving. In *Proceedings of the IEEE/CVF conference on computer vision and pattern recognition*, pages 11621–11631, 2020.
- [5] Mathilde Caron, Piotr Bojanowski, Armand Joulin, and Matthijs Douze. Deep clustering for unsupervised learning of visual features. In *Proceedings of the European Conference on Computer Vision (ECCV)*, pages 132–149, 2018.
- [6] Mathilde Caron, Ishan Misra, Julien Mairal, Priya Goyal, Piotr Bojanowski, and Armand Joulin. Unsupervised learning of visual features by contrasting cluster assignments. *arXiv preprint arXiv:2006.09882*, 2020.
- [7] Ming-Fang Chang, John Lambert, Patsorn Sangkloy, Jagjeet Singh, Slawomir Bak, Andrew Hartnett, De Wang, Peter Carr, Simon Lucey, Deva Ramanan, et al. Argoverse: 3d tracking and forecasting with rich maps. In *Proceedings of the IEEE/CVF Conference on Computer Vision and Pattern Recognition*, pages 8748–8757, 2019.
- [8] Ting Chen, Simon Kornblith, Mohammad Norouzi, and Geoffrey Hinton. A simple framework for contrastive learning of visual representations. In *International conference on machine learning*, pages 1597–1607. PMLR, 2020.
- [9] Xiaozhi Chen, Huimin Ma, Ji Wan, Bo Li, and Tian Xia. Multi-view 3d object detection network for autonomous driving. In *Proceedings of the IEEE Conference on Computer Vision and Pattern Recognition*, pages 1907–1915, 2017.
- [10] Xinlei Chen, Haoqi Fan, Ross Girshick, and Kaiming He. Improved baselines with momentum contrastive learning. *arXiv preprint arXiv:2003.04297*, 2020.
- [11] Yukyung Choi, Namil Kim, Soonmin Hwang, Kibaek Park, Jae Shin Yoon, Kyoungwan An, and In So Kweon. Kaist multi-spectral day/night data set for autonomous and assisted driving. *IEEE Transactions on Intelligent Transportation Systems*, 19(3):934–948, 2018.
- [12] Jia Deng, Wei Dong, Richard Socher, Li-Jia Li, Kai Li, and Li Fei-Fei. Imagenet: A large-scale hierarchical image database. In *2009 IEEE conference on computer vision and pattern recognition*, pages 248–255. Ieee, 2009.
- [13] Mark Everingham, Luc Van Gool, Christopher KI Williams, John Winn, and Andrew Zisserman. The pascal visual object classes (voc) challenge. *International journal of computer vision*, 88(2):303–338, 2010.
- [14] Nils Gähler, Nicolas Jourdan, Marius Cordts, Uwe Franke, and Joachim Denzler. Cityscapes 3d: Dataset and benchmark for 9 dof vehicle detection. *arXiv preprint arXiv:2006.07864*, 2020.
- [15] Yaroslav Ganin and Victor Lempitsky. Unsupervised domain adaptation by backpropagation. In *International conference on machine learning*, pages 1180–1189. PMLR, 2015.
- [16] Andreas Geiger, Philip Lenz, Christoph Stiller, and Raquel Urtasun. Vision meets robotics: The kitti dataset. *The International Journal of Robotics Research*, 32(11):1231–1237, 2013.
- [17] Jakob Geyer, Yohannes Kassahun, Mentar Mahmudi, Xavier Ricou, Rupesh Durgesh, Andrew S Chung, Lorenz Hauswald, Viet Hoang Pham, Maximilian Mühlegg, Sebastian Dorn, et al. A2d2: Audi autonomous driving dataset. *arXiv preprint arXiv:2004.06320*, 2020.
- [18] Jean-Bastien Grill, Florian Strub, Florent Altché, Corentin Tallec, Pierre H Richemond, Elena Buchatskaya, Carl Doersch, Bernardo Avila Pires, Zhaohan Daniel Guo, Mohammad Gheshlaghi Azar, et al. Bootstrapped your own latent: A new approach to self-supervised learning. *arXiv preprint arXiv:2006.07733*, 2020.

- [19] Kaiming He, Haoqi Fan, Yuxin Wu, Saining Xie, and Ross Girshick. Momentum contrast for unsupervised visual representation learning. In *Proceedings of the IEEE/CVF Conference on Computer Vision and Pattern Recognition*, pages 9729–9738, 2020.
- [20] Xinyu Huang, Xinjing Cheng, Qichuan Geng, Binbin Cao, Dingfu Zhou, Peng Wang, Yuanqing Lin, and Ruigang Yang. The apolloscape dataset for autonomous driving. In *Proceedings of the IEEE Conference on Computer Vision and Pattern Recognition Workshops*, pages 954–960, 2018.
- [21] R. Kesten, M. Usman, J. Houston, T. Pandya, K. Nadhamuni, A. Ferreira, M. Yuan, B. Low, A. Jain, P. Ondruska, S. Omari, S. Shah, A. Kulkarni, A. Kazakova, C. Tao, L. Platinsky, W. Jiang, and V. Shet. Lyft level 5 av dataset 2019. <https://level5.lyft.com/dataset/>.
- [22] Jason Ku, Melissa Mozifian, Jungwook Lee, Ali Harakeh, and Steven L Waslander. Joint 3d proposal generation and object detection from view aggregation. In *2018 IEEE/RSJ International Conference on Intelligent Robots and Systems (IROS)*, pages 1–8. IEEE, 2018.
- [23] Samuli Laine and Timo Aila. Temporal ensembling for semi-supervised learning. *arXiv preprint arXiv:1610.02242*, 2016.
- [24] Alex H Lang, Sourabh Vora, Holger Caesar, Lubing Zhou, Jiong Yang, and Oscar Beijbom. Pointpillars: Fast encoders for object detection from point clouds. In *Proceedings of the IEEE/CVF Conference on Computer Vision and Pattern Recognition*, pages 12697–12705, 2019.
- [25] Dong-Hyun Lee et al. Pseudo-label: The simple and efficient semi-supervised learning method for deep neural networks. In *Workshop on challenges in representation learning, ICML*, volume 3, 2013.
- [26] Ming Liang, Bin Yang, Yun Chen, Rui Hu, and Raquel Urtasun. Multi-task multi-sensor fusion for 3d object detection. In *Proceedings of the IEEE/CVF Conference on Computer Vision and Pattern Recognition*, pages 7345–7353, 2019.
- [27] Tsung-Yi Lin, Michael Maire, Serge Belongie, James Hays, Pietro Perona, Deva Ramanan, Piotr Dollár, and C Lawrence Zitnick. Microsoft coco: Common objects in context. In *European conference on computer vision*, pages 740–755. Springer, 2014.
- [28] Mingsheng Long, Yue Cao, Jianmin Wang, and Michael Jordan. Learning transferable features with deep adaptation networks. In *International conference on machine learning*, pages 97–105. PMLR, 2015.
- [29] Yuexin Ma, Xinge Zhu, Sibozhang, Ruigang Yang, Wenping Wang, and Dinesh Manocha. Trafficpredict: Trajectory prediction for heterogeneous traffic-agents. In *Proceedings of the AAAI Conference on Artificial Intelligence*, volume 33, pages 6120–6127, 2019.
- [30] Takeru Miyato, Shin-ichi Maeda, Masanori Koyama, and Shin Ishii. Virtual adversarial training: a regularization method for supervised and semi-supervised learning. *IEEE transactions on pattern analysis and machine intelligence*, 41(8):1979–1993, 2018.
- [31] Mehdi Noroozi and Paolo Favaro. Unsupervised learning of visual representations by solving jigsaw puzzles. In *European conference on computer vision*, pages 69–84. Springer, 2016.
- [32] Abhishek Patil, Srikanth Malla, Haiming Gang, and Yi-Ting Chen. The h3d dataset for full-surround 3d multi-object detection and tracking in crowded urban scenes. In *2019 International Conference on Robotics and Automation (ICRA)*, pages 9552–9557. IEEE, 2019.
- [33] Hieu Pham, Zihang Dai, Qizhe Xie, Minh-Thang Luong, and Quoc V Le. Meta pseudo labels. *arXiv preprint arXiv:2003.10580*, 2020.
- [34] Quang-Hieu Pham, Pierre Sevestre, Ramanpreet Singh Pahwa, Huijing Zhan, Chun Ho Pang, Yuda Chen, Armin Mustafa, Vijay Chandrasekhar, and Jie Lin. A* 3d dataset: Towards autonomous driving in challenging environments. In *2020 IEEE International Conference on Robotics and Automation (ICRA)*, pages 2267–2273. IEEE, 2020.
- [35] Charles R Qi, Wei Liu, Chenxia Wu, Hao Su, and Leonidas J Guibas. Frustum pointnets for 3d object detection from rgb-d data. In *Proceedings of the IEEE conference on computer vision and pattern recognition*, pages 918–927, 2018.
- [36] Shaoshuai Shi, Xiaogang Wang, and Hongsheng Li. Pointcnn: 3d object proposal generation and detection from point cloud. In *Proceedings of the IEEE/CVF Conference on Computer Vision and Pattern Recognition*, pages 770–779, 2019.

- [37] Shaoshuai Shi, Chaoxu Guo, Li Jiang, Zhe Wang, Jianping Shi, Xiaogang Wang, and Hongsheng Li. Pv-rcnn: Point-voxel feature set abstraction for 3d object detection. In *Proceedings of the IEEE/CVF Conference on Computer Vision and Pattern Recognition*, pages 10529–10538, 2020.
- [38] Vishwanath A Sindagi, Yin Zhou, and Oncel Tuzel. Mvx-net: Multimodal voxelnet for 3d object detection. In *2019 International Conference on Robotics and Automation (ICRA)*, pages 7276–7282. IEEE, 2019.
- [39] Kihyuk Sohn, David Berthelot, Chun-Liang Li, Zizhao Zhang, Nicholas Carlini, Ekin D Cubuk, Alex Kurakin, Han Zhang, and Colin Raffel. Fixmatch: Simplifying semi-supervised learning with consistency and confidence. *arXiv preprint arXiv:2001.07685*, 2020.
- [40] Pei Sun, Henrik Kretzschmar, Xerxes Dotiwalla, Aurelien Chouard, Vijaysai Patnaik, Paul Tsui, James Guo, Yin Zhou, Yuning Chai, Benjamin Caine, et al. Scalability in perception for autonomous driving: Waymo open dataset. In *Proceedings of the IEEE/CVF Conference on Computer Vision and Pattern Recognition*, pages 2446–2454, 2020.
- [41] Antti Tarvainen and Harri Valpola. Mean teachers are better role models: Weight-averaged consistency targets improve semi-supervised deep learning results. *arXiv preprint arXiv:1703.01780*, 2017.
- [42] Kai Tian, Shuigeng Zhou, and Jihong Guan. Deepcluster: A general clustering framework based on deep learning. In *Joint European Conference on Machine Learning and Knowledge Discovery in Databases*, pages 809–825. Springer, 2017.
- [43] Sourabh Vora, Alex H Lang, Bassam Helou, and Oscar Beijbom. Pointpainting: Sequential fusion for 3d object detection. In *Proceedings of the IEEE/CVF Conference on Computer Vision and Pattern Recognition*, pages 4604–4612, 2020.
- [44] He Wang, Yezhen Cong, Or Litany, Yue Gao, and Leonidas J Guibas. 3dioumatch: Leveraging iou prediction for semi-supervised 3d object detection. *arXiv preprint arXiv:2012.04355*, 2020.
- [45] Yan Wang, Xiangyu Chen, Yurong You, Li Erran Li, Bharath Hariharan, Mark Campbell, Kilian Q Weinberger, and Wei-Lun Chao. Train in germany, test in the usa: Making 3d object detectors generalize. In *Proceedings of the IEEE/CVF Conference on Computer Vision and Pattern Recognition*, pages 11713–11723, 2020.
- [46] Qizhe Xie, Zihang Dai, Eduard Hovy, Minh-Thang Luong, and Quoc V Le. Unsupervised data augmentation for consistency training. *arXiv preprint arXiv:1904.12848*, 2019.
- [47] Qizhe Xie, Minh-Thang Luong, Eduard Hovy, and Quoc V Le. Self-training with noisy student improves imagenet classification. In *Proceedings of the IEEE/CVF Conference on Computer Vision and Pattern Recognition*, pages 10687–10698, 2020.
- [48] Saining Xie, Jiatao Gu, Demi Guo, Charles R Qi, Leonidas Guibas, and Or Litany. Pointcontrast: Unsupervised pre-training for 3d point cloud understanding. In *European Conference on Computer Vision*, pages 574–591. Springer, 2020.
- [49] Yan Yan, Yuxing Mao, and Bo Li. Second: Sparsely embedded convolutional detection. *Sensors*, 18(10): 3337, 2018.
- [50] Bin Yang, Wenjie Luo, and Raquel Urtasun. Pixor: Real-time 3d object detection from point clouds. In *Proceedings of the IEEE Conference on Computer Vision and Pattern Recognition*, pages 7652–7660, 2018.
- [51] Jihan Yang, Shaoshuai Shi, Zhe Wang, Hongsheng Li, and Xiaojuan Qi. St3d: Self-training for unsupervised domain adaptation on 3d object detection. *arXiv preprint arXiv:2103.05346*, 2021.
- [52] Tianwei Yin, Xingyi Zhou, and Philipp Krähenbühl. Center-based 3d object detection and tracking. *arXiv preprint arXiv:2006.11275*, 2020.
- [53] Jin Hyeok Yoo, Yecheol Kim, Ji Song Kim, and Jun Won Choi. 3d-cvf: Generating joint camera and lidar features using cross-view spatial feature fusion for 3d object detection. *arXiv preprint arXiv:2004.12636*, 3, 2020.
- [54] Fisher Yu, Haofeng Chen, Xin Wang, Wenqi Xian, Yingying Chen, Fangchen Liu, Vashisht Madhavan, and Trevor Darrell. Bdd100k: A diverse driving dataset for heterogeneous multitask learning. In *Proceedings of the IEEE/CVF conference on computer vision and pattern recognition*, pages 2636–2645, 2020.
- [55] Richard Zhang, Phillip Isola, and Alexei A Efros. Colorful image colorization. In *European conference on computer vision*, pages 649–666. Springer, 2016.

- [56] Zaiwei Zhang, Rohit Girdhar, Armand Joulin, and Ishan Misra. Self-supervised pretraining of 3d features on any point-cloud. *arXiv preprint arXiv:2101.02691*, 2021.
- [57] Na Zhao, Tat-Seng Chua, and Gim Hee Lee. Sess: Self-ensembling semi-supervised 3d object detection. In *Proceedings of the IEEE/CVF Conference on Computer Vision and Pattern Recognition*, pages 11079–11087, 2020.
- [58] Yin Zhou and Oncel Tuzel. Voxelnet: End-to-end learning for point cloud based 3d object detection. In *Proceedings of the IEEE Conference on Computer Vision and Pattern Recognition*, pages 4490–4499, 2018.

A The ONCE dataset

We publish the ONCE dataset, benchmark, develop kit, data format and annotation instructions at our website <http://www.once-for-auto-driving.com>. It is our priority to protect the privacy of third parties. We bear all responsibility in case of violation of rights, etc., and confirmation of the data license.

Dataset documentation. <http://www.once-for-auto-driving.com/documentation.html> shows the dataset documentation and intended uses.

Terms of use, privacy and License. The ONCE dataset is published under CC BY-NC-SA 4.0 license, which means everyone can use this dataset for non-commercial research purpose. The detailed Terms of use, privacy terms and license are in http://www.once-for-auto-driving.com/terms_of_use.html.

Data maintenance. <http://www.once-for-auto-driving.com/download.html> provides data download links for users. Data is stored in Google Drive for global users, and another copy of data is stored in BaiduYunPan for Chinese users. We will maintain the data for a long time and check the data accessibility in a regular basis.

Benchmark and code. <http://www.once-for-auto-driving.com/benchmark.html> provides benchmark results. The reproduction code will be released upon acceptance.

Data statistics. Figure 4 shows the proportions of different weather conditions, time periods and areas in the ONCE dataset.

Annotation statistics. Figure 5 shows the distribution of the number of objects for annotated scenes. Our annotated set covers diverse object counts for different scenes, *e.g.* the vehicle count in a scene ranges from less than 1 to more than 50. Pedestrians and cyclists in a scene range from less than 1 to more than 30. The distributions of training, validation and testing splits are mostly similar but slightly different in some intervals, which guarantees stable evaluation results and encourages evaluated methods to have stronger generalizability across the three splits.

Limitations. The major limitation of our ONCE dataset is that currently we only annotate a small amount of scenes of the one million scenes, which may hamper the broader exploration on 3D object detection. To overcome the limitation, we plan to provide more annotations in the near future. We also plan to support more autonomous driving tasks in addition to 3D detection on the ONCE dataset.

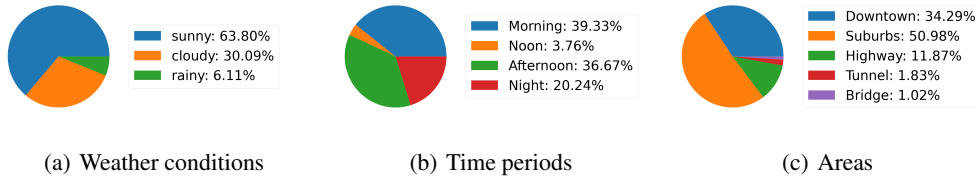


Figure 4: Proportions of different weather, time and areas in the ONCE dataset. Our dataset covers a wide range of domains with 6% scenes captured on rainy days and 20% scenes collected at night.

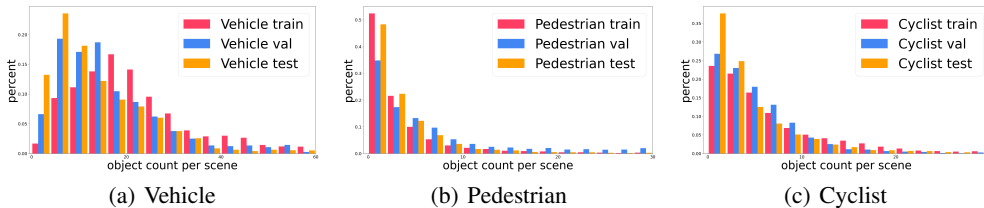


Figure 5: Distribution of annotation counts per scene. Our ONCE dataset is diverse in the number of objects in each scene. The vehicle count in each scene ranges from 0 to 60.

B Experiments

B.1 Models for 3D Object Detection

| Method | Vehicle | | | | Pedestrian | | | | Cyclist | | | | mAP |
|--|---------|-------|--------|---------|------------|-------|--------|---------|---------|-------|--------|---------|-------|
| | overall | 0-30m | 30-50m | 50m-inf | overall | 0-30m | 30-50m | 50m-inf | overall | 0-30m | 30-50m | 50m-inf | |
| Multi-Modality (point clouds + images) | | | | | | | | | | | | | |
| PointPainting [43] | 66.17 | 80.31 | 59.80 | 42.26 | 44.84 | 52.63 | 36.63 | 22.47 | 62.34 | 73.55 | 57.20 | 40.39 | 57.78 |
| Single-Modality (point clouds only) | | | | | | | | | | | | | |
| PointRCNN [36] | 52.09 | 74.45 | 40.89 | 16.81 | 4.28 | 6.17 | 2.40 | 0.91 | 29.84 | 46.03 | 20.94 | 5.46 | 28.74 |
| PointPillars [24] | 68.57 | 80.86 | 62.07 | 47.04 | 17.63 | 19.74 | 15.15 | 10.23 | 46.81 | 58.33 | 40.32 | 25.86 | 44.34 |
| SECOND [49] | 71.19 | 84.04 | 63.02 | 47.25 | 26.44 | 29.33 | 24.05 | 18.05 | 58.04 | 69.96 | 52.43 | 34.61 | 51.89 |
| PV-RCNN [37] | 77.77 | 89.39 | 72.55 | 58.64 | 23.50 | 25.61 | 22.84 | 17.27 | 59.37 | 71.66 | 52.58 | 36.17 | 53.55 |
| CenterPoints [52] | 66.79 | 80.10 | 59.55 | 43.39 | 49.90 | 56.24 | 42.61 | 26.27 | 63.45 | 74.28 | 57.94 | 41.48 | 60.05 |

Table 9: Results of detection models on the validation split.

B.2 Self-Supervised Learning for 3D Object Detection

| Method | Vehicle | | | | Pedestrian | | | | Cyclist | | | | mAP |
|--------------------|---------|-------|--------|---------|------------|-------|--------|---------|---------|-------|--------|---------|---------------|
| | overall | 0-30m | 30-50m | 50m-inf | overall | 0-30m | 30-50m | 50m-inf | overall | 0-30m | 30-50m | 50m-inf | |
| baseline [49] | 71.19 | 84.04 | 63.02 | 47.25 | 26.44 | 29.33 | 24.05 | 18.05 | 58.04 | 69.96 | 52.43 | 34.61 | 51.89 |
| U_{small} | | | | | | | | | | | | | |
| BYOL [18] | 68.02 | 81.01 | 60.21 | 44.17 | 19.50 | 22.16 | 16.68 | 12.06 | 50.61 | 62.46 | 44.29 | 28.18 | 46.04 (-5.85) |
| PointContrast [48] | 71.07 | 83.31 | 64.90 | 49.34 | 22.52 | 23.73 | 21.81 | 16.06 | 56.36 | 68.11 | 50.35 | 34.06 | 49.98 (-1.91) |
| SwAV [6] | 72.71 | 83.68 | 65.91 | 50.10 | 25.13 | 27.77 | 22.77 | 16.36 | 58.05 | 69.99 | 52.23 | 34.86 | 51.96 (+0.07) |
| DeepCluster [42] | 73.19 | 84.25 | 66.86 | 50.47 | 24.00 | 26.36 | 21.73 | 16.79 | 58.99 | 70.80 | 53.66 | 36.17 | 52.06 (+0.17) |
| U_{medium} | | | | | | | | | | | | | |
| BYOL [18] | 70.93 | 84.15 | 63.48 | 45.74 | 25.86 | 29.91 | 21.55 | 15.83 | 55.63 | 58.59 | 49.01 | 29.53 | 50.82 (-1.07) |
| PointContrast [48] | 71.39 | 83.89 | 65.22 | 47.73 | 27.69 | 32.53 | 23.00 | 14.68 | 56.88 | 69.01 | 50.41 | 34.57 | 51.99 (+0.10) |
| SwAV [6] | 72.51 | 83.39 | 65.46 | 51.08 | 27.08 | 29.94 | 25.19 | 17.13 | 57.85 | 69.87 | 52.38 | 33.78 | 52.48 (+0.59) |
| DeepCluster [42] | 71.62 | 83.99 | 65.55 | 50.77 | 29.33 | 33.25 | 25.08 | 17.00 | 57.61 | 68.57 | 52.58 | 34.05 | 52.86 (+0.97) |
| U_{large} | | | | | | | | | | | | | |
| BYOL [18] | 71.32 | 83.59 | 64.89 | 50.27 | 25.02 | 27.06 | 22.96 | 17.04 | 58.56 | 70.18 | 52.74 | 36.32 | 51.63 (-0.26) |
| PointContrast [48] | 71.87 | 86.93 | 62.85 | 48.65 | 28.03 | 33.07 | 25.91 | 14.44 | 60.88 | 71.12 | 55.77 | 36.78 | 53.59 (+1.70) |
| SwAV [6] | 72.46 | 83.09 | 66.66 | 51.50 | 29.84 | 34.15 | 26.22 | 17.61 | 57.84 | 68.79 | 52.21 | 35.39 | 53.38 (+1.49) |
| DeepCluster [42] | 72.89 | 83.52 | 67.09 | 50.38 | 30.32 | 34.76 | 26.43 | 18.33 | 57.94 | 69.18 | 52.42 | 34.36 | 53.72 (+1.83) |

Table 10: Results of self-supervised learning methods on the validation split.

B.3 Semi-Supervised Learning for 3D Object Detection

| Method | Vehicle | | | | Pedestrian | | | | Cyclist | | | | mAP |
|--------------------|---------|-------|--------|---------|------------|-------|--------|---------|---------|-------|--------|---------|---------------|
| | overall | 0-30m | 30-50m | 50m-inf | overall | 0-30m | 30-50m | 50m-inf | overall | 0-30m | 30-50m | 50m-inf | |
| baseline [49] | 71.19 | 84.04 | 63.02 | 47.25 | 26.44 | 29.33 | 24.05 | 18.05 | 58.04 | 69.96 | 52.43 | 34.61 | 51.89 |
| U_{small} | | | | | | | | | | | | | |
| Pseudo Label [25] | 72.80 | 84.46 | 64.97 | 51.46 | 25.50 | 28.36 | 22.66 | 18.51 | 55.37 | 65.95 | 50.34 | 34.42 | 51.22 (-0.67) |
| Noisy Student [47] | 73.69 | 84.69 | 67.72 | 53.41 | 28.81 | 33.23 | 23.42 | 16.93 | 54.67 | 65.58 | 50.43 | 32.65 | 52.39 (+0.50) |
| Mean Teacher [41] | 74.46 | 86.65 | 68.44 | 53.59 | 30.54 | 34.24 | 26.31 | 20.12 | 61.02 | 72.51 | 55.24 | 39.11 | 55.34 (+3.45) |
| SESS [57] | 73.33 | 84.52 | 66.22 | 52.83 | 27.31 | 31.11 | 23.94 | 19.01 | 59.52 | 71.03 | 53.93 | 36.68 | 53.39 (+1.50) |
| 3DIoUMatch [44] | 73.81 | 84.61 | 68.11 | 54.48 | 30.86 | 35.87 | 25.55 | 18.30 | 56.77 | 68.02 | 51.80 | 35.91 | 53.81 (+1.92) |
| U_{medium} | | | | | | | | | | | | | |
| Pseudo Label [25] | 73.03 | 86.06 | 65.96 | 51.42 | 24.56 | 27.28 | 20.81 | 17.00 | 53.61 | 65.26 | 48.44 | 33.58 | 50.40 (-1.49) |
| Noisy Student [47] | 75.53 | 86.52 | 69.78 | 55.05 | 31.56 | 35.80 | 26.24 | 21.21 | 58.93 | 69.61 | 53.73 | 36.94 | 55.34 (+3.45) |
| Mean Teacher [41] | 76.01 | 86.47 | 70.34 | 55.92 | 35.58 | 40.86 | 30.44 | 19.82 | 63.21 | 74.89 | 56.77 | 40.29 | 58.27 (+6.38) |
| SESS [57] | 72.11 | 84.06 | 66.44 | 53.61 | 33.44 | 38.58 | 28.10 | 18.67 | 61.82 | 73.20 | 56.60 | 38.73 | 55.79 (+3.90) |
| 3DIoUMatch [44] | 75.69 | 86.46 | 70.22 | 56.06 | 34.14 | 38.84 | 29.19 | 19.62 | 58.93 | 69.08 | 54.16 | 38.87 | 56.25 (+4.36) |
| U_{large} | | | | | | | | | | | | | |
| Pseudo Label [25] | 72.41 | 84.06 | 64.54 | 50.05 | 23.62 | 26.80 | 20.13 | 16.66 | 53.25 | 64.69 | 48.52 | 33.47 | 49.76 (-2.13) |
| Noisy Student [47] | 75.99 | 86.67 | 70.48 | 55.60 | 33.31 | 37.81 | 28.19 | 21.39 | 59.81 | 70.01 | 55.13 | 38.33 | 56.37 (+4.48) |
| Mean Teacher [41] | 76.38 | 86.45 | 70.99 | 57.48 | 35.95 | 41.76 | 29.05 | 18.81 | 65.50 | 75.72 | 60.07 | 43.66 | 59.28 (+7.39) |
| SESS [57] | 75.95 | 86.83 | 70.45 | 55.76 | 34.43 | 40.00 | 27.92 | 19.20 | 63.58 | 74.85 | 58.88 | 39.51 | 57.99 (+6.10) |
| 3DIoUMatch [44] | 75.81 | 86.11 | 71.82 | 57.84 | 35.70 | 40.68 | 30.34 | 21.15 | 59.69 | 70.69 | 54.92 | 39.08 | 57.07 (+5.18) |

Table 11: Results of semi-supervised learning methods on the validation split.

C Implementation details

In this section, we provide implementation and training details for the 3D object detection benchmark.

C.1 Models for 3D Object Detection

Data split. We use the training split to train those 6 models. The performance is evaluated on the validation and testing split.

General configurations. Non Maximum Suppression (NMS) with the IoU threshold 0.01 is adopted for post-processing. Other configurations are kept the same with the official version of those models if not specially mentioned.

Learning scheme. All the 6 models are trained with an initial learning rate 0.003 under the cosine annealing learning scheme. We use the adam optimizer for all the models. The models are trained with the batch size 32 for 80 epochs.

Data augmentation. For all the models, we use random flip of the X and Y axis, random rotation from -45° to $+45^\circ$, random scaling from 0.95 to 1.05, and objects cut and paste on the input point cloud as augmentations. We didn't apply augmentations on segmentation maps for PointPainting.

PointRCNN. PointRCNN is a point-based 3D detector that generates proposals directly on point clouds. We sample 60000 points per frame and construct the segmentation backbone with 32000-4000-500-256 points. We use the mean size of each category for proposal generation.

PointPillars. PointPillars is a pioneering work that introduces pillar-based representation into 3D object detection. We set the pillar size as $0.2m \times 0.2m$ and also use the mean size as the anchor size.

SECOND. SECOND is a voxel-based detector that transforms point clouds into voxels for feature extraction. We set the voxel size as $0.1m \times 0.1m \times 0.2m$ and use the same anchors as PointPillars.

PV-RCNN. PV-RCNN is a point-voxel based detector that applies SECOND for proposal generation and then utilizes keypoints for RoI feature extraction. We sample 4096 keypoints per scene.

CenterPoints. CenterPoints introduces center-based target assignments to replace the anchor-based assignments. In addition to the center head, we use the same backbone as SECOND.

PointPainting. PointPainting uses CenterPoints as the 3D detector and HRNet trained on CityScapes to generate semantic segmentation results.

C.2 Self-Supervised Learning for 3D Object Detection

Data split. We conduct self-supervised pretraing on the unlabeled sets U_* and then use the training split to finetune models. The performance is evaluated on the validation and testing split.

General configurations. We use the voxel-based SECOND detector as the baseline model for all the methods. During the pretraining stage, we pretrain the backbone of SECOND detector on unlabeled subset. We pretrain those methods for 20 epochs on the 100k unlabeled subset U_{small} , 5 epochs on the 500k subset U_{medium} and 3 epochs on the 1 million subset U_{large} .

Learning scheme. For all the methods, the pretaining and finetuning learning rate is initialized as 0.003. We use the adam optimizer and the cosine annealing learning scheme for all the methods.

Multi-view augmentation setup. We generate multi-view of the original scenes by random flip, scaling with a scale factor sampled from [0.95, 1.05] and rotation around vertical yaw axis between [-10, 10] degrees. We also do downsampling by a factor sampled from [0.9, 1].

PointContrast. PointContrast defines a contrastive loss over the point-level features given a pair of overlapping partial scans. The objective is to minimize the distance between matched points (positive pairs) and maximize the distance between unmatched ones (negative pairs). In our setting, we sample a random geometric transformation to transform an original point cloud scene into 2 augmented views. After passing the scenes through SECOND backbone to obtain voxel-wise features, we randomly select 1024 voxels within each scene. The voxel-wise features will be passed through a two-layer MLP (with dimension 128, 64) to project into latent space, with batchnorm and ReLU. The latent space feature will be concatenated with initial feature and passed through a one-layer MLP with

dimension 64. The final features will be used for contrastive pretraining. We pretrain the model using Adam optimizer with the initial learning rate 0.001 and the batch size as 4.

DeepCluster. DeepCluster uses k-means clustering to give each instance a cluster id as the pseudo label and use the label to train the network. Since clustering method is designed to learn semantic representation, we randomly crop patches in 3D scenes as pseudo instances and pass the patches through the backbone to obtain patch-wise features. We project the features into latent space for clustering and pretraining. We choose the total cluster number as 100. Patch-wise feature will be passed through a two-layer MLP (with dimension 192, 128), with a batchnorm and ReLU layer to project the features to the latent space. This two-layer MLP will not be used in the finetune stage. We pretrain the backbone with Adam optimizer. The initial learning rate is 0.0048 with a cosine decay. The batch size is 256.

SwAV. SwAV improves DeepCluster by introducing prototypes, online clustering and swapped predictions. We use the same clustering and training settings as DeepCluster. For other configurations we follow the settings in the original paper.

BYOL. BYOL introduces two networks, referred to online network and target network, that can interact and learn from each other. Given a 3D scene, we train the online network to predict the target network’s representation of an augmented view of the same scene. In particular, after passing the 3D scene through the backbone, we project the representation through a two-layer MLP (with dimension 4096, 512). After that, the predictor in the online network will project the embedding into a latent space as the final representation of the online network. The predictor is also a two-layer MLP (with dimension 4096, 512). We update the target network by a slow-moving averaging of the online network with parameter 0.999. To avoid the model collapsing to trivial solutions, we further introduce a contrastive regularization term. Specifically, we follow the design in PointContrast and randomly select some voxel-wise features. A contrastive loss is designed on different views of the same voxel between its online representation and target representation. We pretrain the model using Adam optimizer with the initial learning rate 0.001. The batch size is 4.

C.3 Semi-Supervised Learning for 3D Object Detection

Data split. We first utilize the training split to obtain pretrained teacher and student models, and then we apply semi-supervised learning on the unlabeled set U_* . The performance is evaluated on the validation and testing split.

General configurations. We use the SECOND detector as the baseline model for all the methods, which guarantees a fair comparison among those methods. The pretraining process and configurations follow those in C.1.

Learning scheme. The initial learning rate is 0.003 for both the pretraining and semi-supervised learning process. We use the adam optimizer and the cosine annealing learning scheme for all the methods. For pretraining, the batch size is 32. For semi-supervised learning, the batch size of labeled data is 8 and the batch size of unlabeled data is 32. The pretraining process lasts 80 epochs. The semi-supervised learning process lasts 25 epochs for U_{small} and 5 epochs for U_{medium} and U_{large} .

Data augmentation. During the pretraining process, we use random flip of the X and Y axis, random rotation from -45° to $+45^\circ$, random scaling from 0.95 to 1.05, and objects cut and paste on the input point cloud as augmentations. During the semi-supervised learning process, we use the same random flip, random rotation and random scaling for the student model. We didn’t apply augmentations on the teacher model.

Pseudo Label. We use the pretrained model to generate pseudo ground truth boxes for each unlabeled scene. The model is then trained with pseudo labels in the unlabeled scenes, as well as real labels in the training split. It is worth noting that we didn’t apply any augmentation in the semi-supervised learning process, mainly to explore whether augmentations are necessary with a large amount of data.

Mean Teacher. Mean Teacher uses the teacher and student model for semi-supervised learning. We first load the pretrained weights for both two models, and then the teacher model produces pseudo ground truths to train the student model for the unlabeled subset. A consistency loss is introduced to regularize two models. Specifically, we first match the predicted boxes of student model with pseudo boxes of teacher model by the nearest-neighbor criterion. Then the Kullback–Leibler divergence of

class predictions of the matched pairs of boxes is applied as the consistency loss. The teacher model is updated by exponential moving average (EMA) of the student model.

Noisy Student. Noisy Student is a self-training approach in which the student is trained with noise, *i.e.*, strong augmentations, using pseudo labels provided by the teacher. After the first round of semi-supervised training, we make the student a new teacher for the second round.

SESS. Self-Ensembling Semi-Supervised (SESS) 3D object detection extends Mean Teacher by introducing another two consistency constraints: size consistency and center consistency, along with class consistency to the matched pairs of boxes. The teacher is also updated by EMA.

3DIoUMatch. 3DIoUMatch introduces an extra IoU prediction head on the detection model. The predicted IoUs are then used for filtering low-quality pseudo boxes. We reject IoU-guided lower-half suppression and the EMA update scheme, since those components are detrimental to the detection performance in our experiments.

C.4 Unsupervised Domain Adaptation for 3D Object Detection

Data split. We conduct unsupervised domain adaptation on the training split. The performance is evaluated on the validation split.

Learning scheme. We completely follow the same learning rate, optimizer and learning scheme used in [51].

Data augmentation. We completely follow the augmentations used in [51].

SN. Statistical Normalization (SN) is based on the observation that domain gap mainly comes from the differences of object size between different datasets, so this method normalizes the objects' size of the source dataset according to the object statistics on the target domain.

ST3D. ST3D contains two stages: the model is first trained on the source dataset with an augmentation method named random object scaling. Then the model is trained on the target dataset with the aid of pseudo labels and a memory bank.

D Visualization

Annotation example. We present an example of annotations in Figure 6.

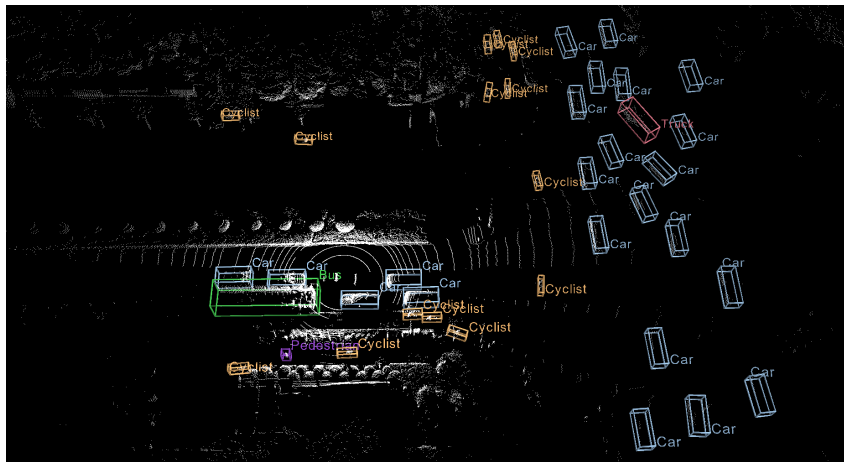


Figure 6: Example of 3D annotations.

3D annotations for RGB images. We present an example of 3D annotations on an RGB image in Figure 7.

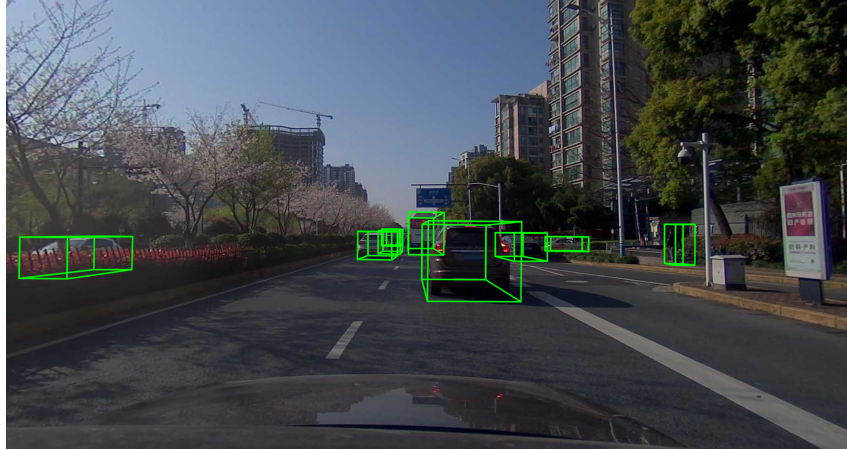


Figure 7: Example of 3D annotations on an RGB image.

Multi-modality alignments. We present an illustration of the alignments between point clouds and images in Figure 8.

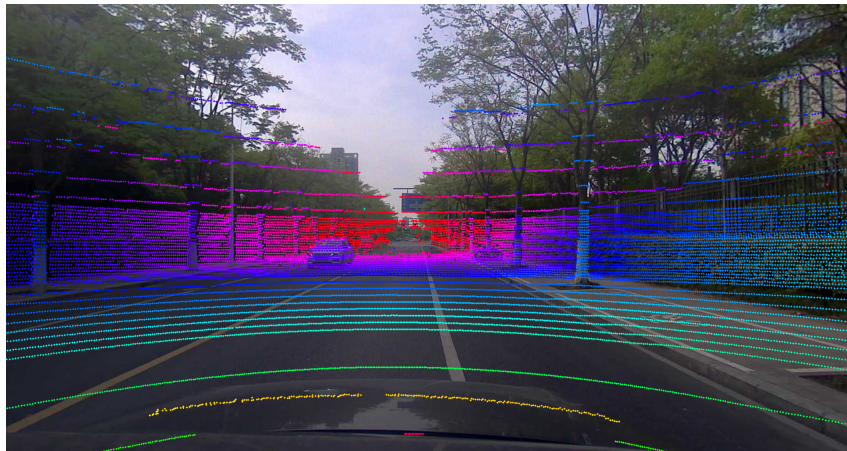


Figure 8: Alignment of point cloud and image.

Annotation system. We present an interface of the annotation system in Figure 9.

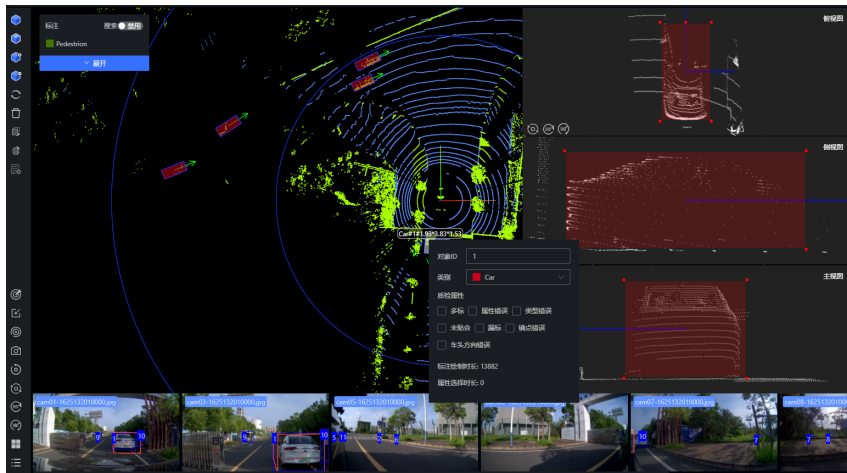


Figure 9: Annotation system.

E Evaluation Metric

Evaluation metric is critical for fair comparisons of different approaches on 3D object detection. Current 3D IoU-based evaluation metric AP_{3D} [16] faces the problem that objects with opposite orientations can both be matched to the ground truth with the IOU criterion. To resolve this problem, we extend [16] and take the object orientations into special consideration. In particular, we first re-rank the predictions according to their scores, and set those predicted boxes that have low 3D IoUs with all ground truths of the same category as false positives. The IoU thresholds are 0.7, 0.7, 0.7, 0.3, 0.5 for car, bus, truck, pedestrian, cyclist respectively. Then we add additional filtering step in which we also set those predictions as false positives if their orientations θ cannot fall into the $\pm 90^\circ$ range of the matched ground truth orientations θ' . This step sets a more stringent criterion specially for orientations. The remaining matched predictions are treated as true positives. Finally, we determine 50 score thresholds with the recall rates r from 0.02 to 1.00 at the step 0.02 and we calculate the corresponding 50 precision rates to draw the precision-recall curve $p(r)$. The calculation of our orientation-aware AP_{3D}^{Ori} can be formulated as:

$$AP_{3D}^{Ori} = 100 \int_0^1 \max\{p(r' | r' \geq r)\} dr. \quad (1)$$

We merge the car, bus and truck class into a super-class called vehicle following [40], so we officially report the AP_{3D}^{Ori} of vehicle, pedestrian and cyclist respectively in the following experiments. We still provide the evaluation interface of 5 classes for users. Mean AP (mAP) is thus obtained by averaging the scores of 3 categories. To further inspect the detection performance of different distances, we also provide AP_{3D}^{Ori} of 3 distance ranges: within 30m, 30-50m, and farther than 50m. This is obtained by only considering ground truths and predictions within that distance range.

Discussion on different evaluation metrics. Current evaluation metrics of 3D detection typically extend the Average Precision (AP) metric [13] of 2D detection to the 3D scenarios by changing the matching criterion between the ground truth boxes and predictions. The nuScenes dataset [4] uses the center distance between boxes on the ground plane as the matching criterion for AP calculation, in ignorance of the size and orientation of the objects. Although the nuScenes detection score (NDS) is proposed to take all factors into consideration, AP still accounts for 50% of the total NDS score, which shows strong preference to the accurate localization of object centers but less attention to the objects' size and orientation. The Waymo Open dataset [40] applies the Hungarian algorithm to match the ground truths and predictions, which may lead to a higher estimation of AP since objects with no overlaps can also be matched. The KITTI dataset [16] uses 3D Intersection over Union (IoU) above certain threshold as the matching criterion, but the predicted boxes with the opposite orientations of the ground truths can also be matched, which can be dangerous in practical. In this paper, we extend the 3D IoU-based evaluation metric AP of [16] and take the object orientations into special consideration. Our orientation-aware AP_{3D}^{Ori} metric is more stringent than [16]. Compared with the weighted-scoring method in [40], our method avoids repeated calculations of the orientation factor, since it has already participated in the computation of 3D rotated IoU. Compared with the distance-based matching scheme [4], our method puts equal weights on the object size, center and orientation.